Seasonal variation of a coastal jet in the Long Island Sound outflow region based on HF radar and Doppler current observations

D. S. Ullman
Graduate School of Oceanography, University of Rhode Island, Narragansett, Rhode Island, USA

D. L. Codiga
Department of Marine Sciences, University of Connecticut, Groton, Connecticut, USA

Received 26 September 2002; revised 12 May 2003; accepted 21 May 2003; published 5 June 2004.

[1] Surface current (HF radar) and velocity profile observations, obtained as part of the Front-Resolving Observational Network with Telemetry (FRONT) project over an approximately 2-year period, are used to describe the seasonal variability of a coastal jet in the Long Island Sound outflow region. The jet is observed in an area of the continental shelf where surface thermal fronts are frequently detected during both summer and winter. The current jet is coincident with a band of high summer frontal probability, and apparently arises from the interaction between Long Island Sound outflow and larger-scale alongshore currents on the shelf. The jet reaches peak strength in summer (transport of $\sim$0.07 Sv) and is weak or non-existent in winter. Flow is strongest near the surface and weakens with depth, with only moderate seasonal variations in the vertical shear. The relatively long data set of currents combined with historical hydrographic measurements and buoy wind observations is analyzed to examine the seasonal variability of the terms in the depth-averaged momentum balance. The depth-averaged pressure gradient is partitioned into a steric component, evaluated from the hydrography, and a non-steric component that is estimated as the residual of the computed terms in the momentum equation. The depth-averaged momentum balance is found to be approximately geostrophic in the across-shore direction. The seasonal variability in the jet arises due to the shifting balance between buoyancy-driven flow that is always downshelf but intensifies somewhat in summer and wind-driven flow which dominates in winter when wind stress becomes strongly upwelling favorable. *INDEX TERMS:* 4219 Oceanography: General: Continental shelf processes; 4227 Oceanography: General: Diurnal, seasonal, and annual cycles; 4223 Oceanography: General: Descriptive and regional oceanography; 4512 Oceanography: Physical: Currents; *KEYWORDS:* FRONT, coastal jet, HF radar, Doppler current, Long Island Sound

Citation: Ullman, D. S., and D. L. Codiga (2004), Seasonal variation of a coastal jet in the Long Island Sound outflow region based on HF radar and Doppler current observations, *J. Geophys. Res.*, *109*, C07S06, doi:10.1029/2002JC001660.

1. Introduction

[2] Surface thermal fronts are frequently observed during summer and winter over the inner continental shelf in the region influenced by the outflow from Long Island/Block Island Sounds [*Ullman and Cornillon*, 1999]. This area has been the focus of the observation/modeling project Front-Resolving Observational Network with Telemetry (FRONT, www.nopp.uconn.edu), with both remote sensing (HF radar, AVHRR, SeaWiFS) and in situ (moored ADCP, CTD) observational components (Figure 1). The objective of the project was to couple real-time, multiplatform observations with a 3-dimensional numerical model to provide the oceanographic description of, and predictive capability for, an approximately 1500 km^2 shelf region. The current data obtained as part of this project represent a relatively long record and are exploited, in this paper, to examine seasonal variability in coastal circulation.

[3] The Middle Atlantic Bight shelf is probably one of the most well-studied continental shelf regions in the world, with early studies, reviewed by *Beardsley and Boicourt* [1981], indicating a mean downshelf (southwestward) flow increasing offshore toward the shelfbreak. Strong synoptic-scale temporal variability in flows on this shelf has been mainly attributed to wind forcing [*Beardsley and Butman*, 1974; *Chuang et al.*, 1979; *Mayer et al.*, 1979; *Beardsley et al.*, 1985]. On seasonal timescales, however, the generally accepted view, based largely on observations from the Nantucket Shoals Flux Experiment [*Beardsley et al.*, 1985] over a full year, is that the flow over the middle and outer shelf is fairly steady. Here we examine a region of

0148-0227/04/2002JC001660

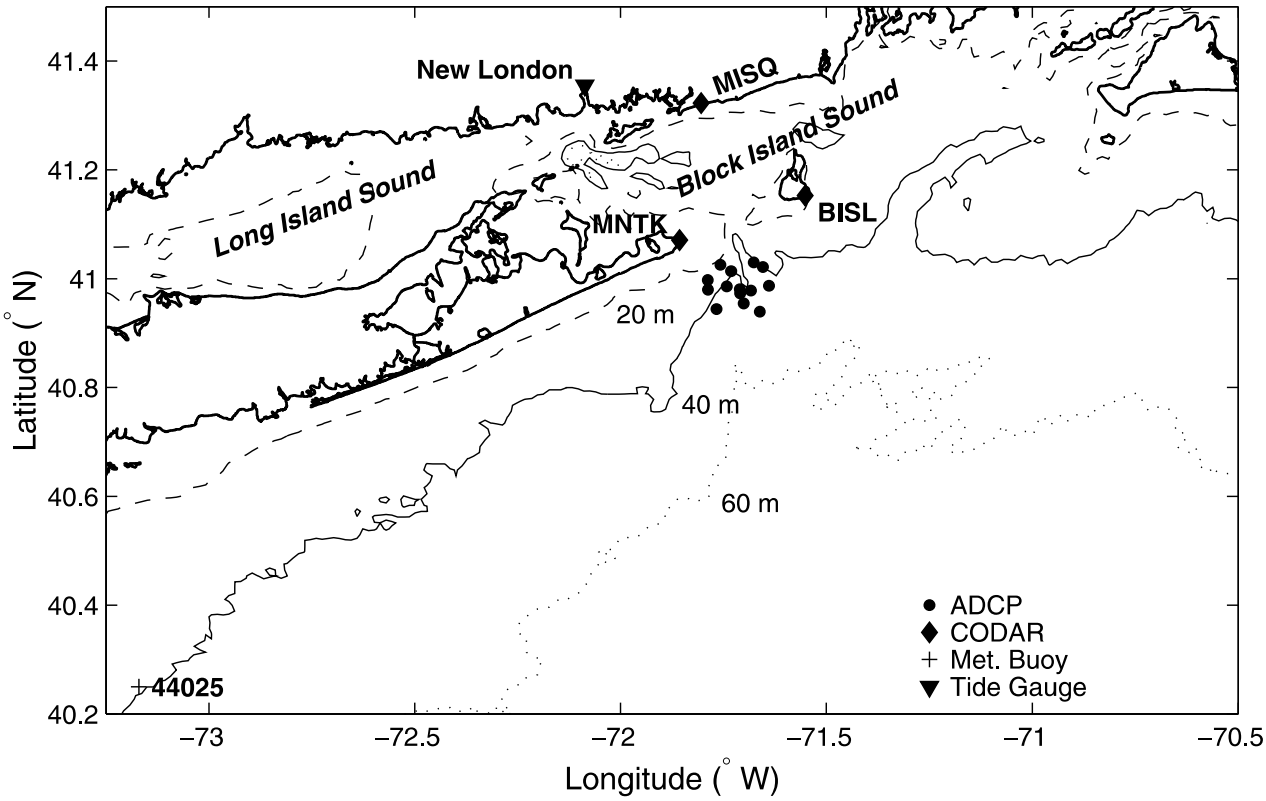

Figure 1. Front-Resolving Observational Network with Telemetry region of interest. CODAR sites at Block Island (BISL), Misquamicut (MISQ), and Montauk Point (MNTK) are shown along with locations at which ADCPs were located during 2000–2001. Wind data were obtained from buoy 44025, and water level observations from New London were also utilized.

the inner shelf where, in contrast, the dynamics exhibits strong seasonal variability due to variations in estuarine outflow and in wind stress over seasonal timescales.

[4] The continental shelf south of Montauk Point, Long Island, receives the outflow from Long Island Sound via Block Island Sound. The freshwater flux from Long Island Sound is primarily due to the Connecticut River ($\sim$500 m^3/s long-term mean) located near the estuary mouth about 20 km west of New London (Figure 1). On the basis of observations of gravitational circulation in the western sound [*Wilson*, 1976], the Hudson River drainage likely contributes a substantial amount of freshwater to the western end. Strong tidal currents and associated vertical mixing occur in the race at the mouth of Long Island Sound and in Block Island Sound in the vicinity of Montauk Point [*Bowman and Esaias*, 1981].

[5] Sea surface temperature (SST) fronts over the mid-Atlantic Bight shelf appear frequently during winter in a well-defined mid-shelf band extending from Nova Scotia to Cape Hatteras and centered roughly over the 50-m isobath, distinct from and inshore of the shelfbreak front [*Ullman and Cornillon*, 1999]. Although detected in SST, these winter fronts are more strongly controlled by salinity with fresher, cooler, and less dense water inshore [*Ullman and Cornillon*, 2001]. In summer, surface thermal fronts are less widespread occurring in the strongly tidal waters of Georges Bank, the Gulf of Maine, and in the Block Island Sound outflow region. The probability of detecting an SST front during July and January in the FRONT region is shown in Figure 2. In summer (July), fronts are found in a narrow band extending from northeast of Block Island southwestward past Montauk Point. In winter (January), the high-probability band is wider in the cross-shelf direction and, as mentioned above, is part of a larger-scale coastal frontal zone [*Ullman and Cornillon*, 1999].

[6] The focus of this paper is the seasonal variability and dynamics of a current jet that is observed coincident with the frontal zone southwest of Block Island. The characteristics of the jet are presented using a combination of HF radar-derived surface currents and bottom-mounted current profilers in the frontal zone. Historical hydrography is used to construct a mean seasonal density field allowing estimation of the depth-averaged baroclinic forcing. Analysis of the quasi-steady momentum balance within the frontal zone then quantifies the processes responsible for the observed seasonal variability of the jet.

2. Measurements and Methods

2.1. HF Radar Currents

[7] Surface currents were measured with a three-site network of SeaSonde systems (marketed by CODAR Ocean Sensors) located at Montauk Point on the eastern tip of Long Island, Block Island, and on the southern Rhode Island coast at Misquamicut (Figure 1). The SeaSondes operated at $\sim$25 MHz with cell size of 1.5 km in range and

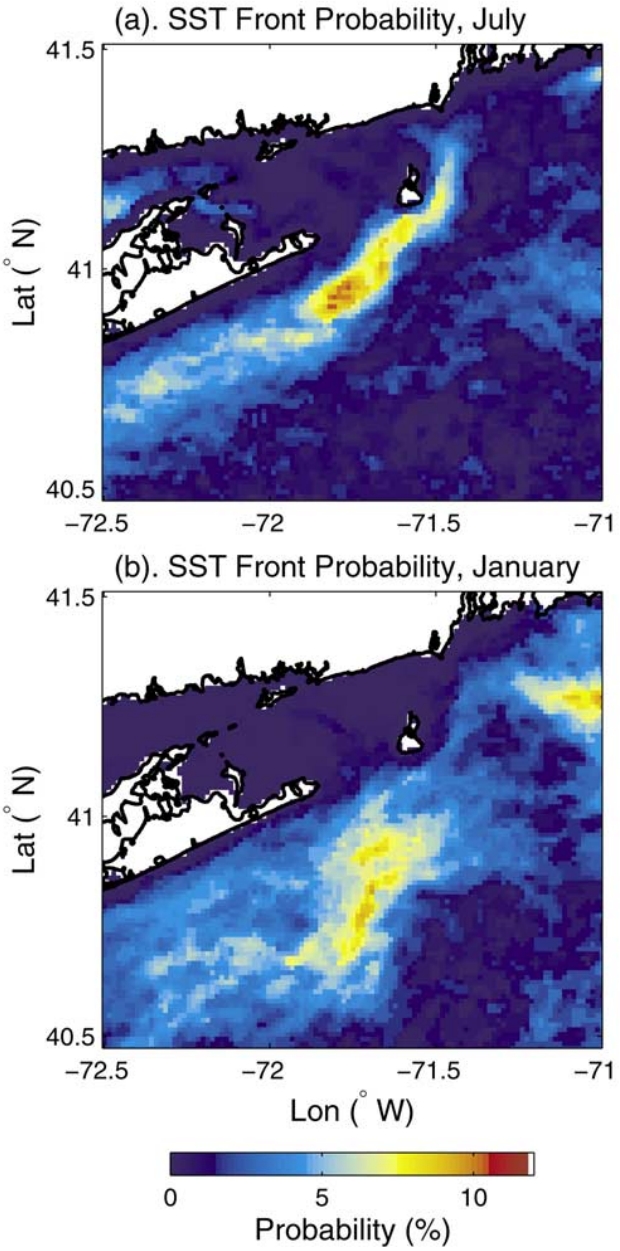

Figure 2. Probability of detecting an SST front during (a) July and (b) January, averaged over 1985–1996.

5° in azimuth and were configured to provide hourly averaged radial currents, which were subsequently combined, in the regions of overlapping coverage from two or more sites, to produce hourly vector currents. The analysis described in this paper utilizes 19 months of surface current observations from June 2000 to December 2001.

[8] The basic principles underlying the estimation of surface currents from HF radar backscatter have been well described in the literature [*Barrick et al.*, 1974; *Stewart and Joy*, 1974; *Barrick et al.*, 1977], and will not be repeated here. At 25 MHz, the radar-derived surface current represents an average over the upper 0.5 m of the water column [*Stewart and Joy*, 1974]. The SeaSonde utilizes a colocated three-element receive antenna array and direction-finding techniques to invert radar backscatter to determine surface currents. The reader is referred to *Lipa and Barrick* [1983] and *Barrick and Lipa* [1997] for details of the direction-finding algorithm. Receive antenna patterns were measured with a transponder at the start of the deployment and again more than a year later and were found to be substantially similar. Corrections for the measured distortion from ideality of the antenna pattern were performed at each radial site during processing [*Barrick and Lipa*, 1986]. From comparisons with ADCP near-surface currents and a radar-radar comparison along the baseline between Montauk and Misquamicut (Figure 1), the error in hourly radial velocity is estimated to be 0.07–0.12 m/s (D. S. Ullman et al., Evaluation of CODAR radial velocity errors using baseline comparisons and ADCP data, manuscript in preparation, 2004) (hereinafter referred to as Ullman et al., manuscript in preparation, 2004).

[9] Estimation of vector currents from the measured radials followed a modified version of the least squares technique described by *Lipa and Barrick* [1983]. At a particular position, the eastward and northward velocity components are computed as the parameters of a least squares fit to all radial velocities located within a 2.5-km radius. Assuming known (constant) radial velocity errors, the standard deviation in the least squares estimated velocity components is easily derived [*Press et al.*, 1992] and depends only on the geometry of the radials and the number of radials used in the fit [*Lipa and Barrick*, 1983; *Chapman et al.*, 1997]. It is generally time variable because the inverse nature of the radial site direction finding algorithm can result in coverage gaps; that is, all radial velocity cells from a particular site are not necessarily filled each hour. For this reason, standard deviation maps are computed for each hour, assuming that radial velocity errors from all sites are constant in space and time. For Block Island, Misquamicut, and Montauk, radial velocity standard errors of 0.12, 0.11, and 0.07 m/s, respectively, estimated by Ullman et al. (manuscript in preparation, 2004), are used in this calculation. The median value of the standard deviation, computed over the entire 19-month period, is used to show the typical magnitude of the errors in the vector components (Figure 3). The errors are 0.06 m/s or less in the central part of the domain and increase rapidly toward the edges of the coverage area due to a reduction in the number of available radials and to increasingly non-optimal geometry. Note also that errors in the eastward component increase in the vicinity of the baseline between the Montauk and Misquamicut sites because at these locations both sites measure essentially the same (north) component of velocity.

[10] Temporal data coverage was quantified by computing the percent of total possible vector returns at each CODAR grid point (Figure 4). Percent coverage decreases rapidly near the edges of the domain where least squares vector errors are large. For this reason, a threshold on percent coverage was used to screen out CODAR grid points where data were less reliable. Time series of east and north surface currents at grid points with percent coverage greater than 50% were harmonically analyzed at tidal frequencies and low-pass filtered using a fourth order Butterworth filter with a cutoff period of 36 hours. Missing data values were replaced by the record mean value prior to

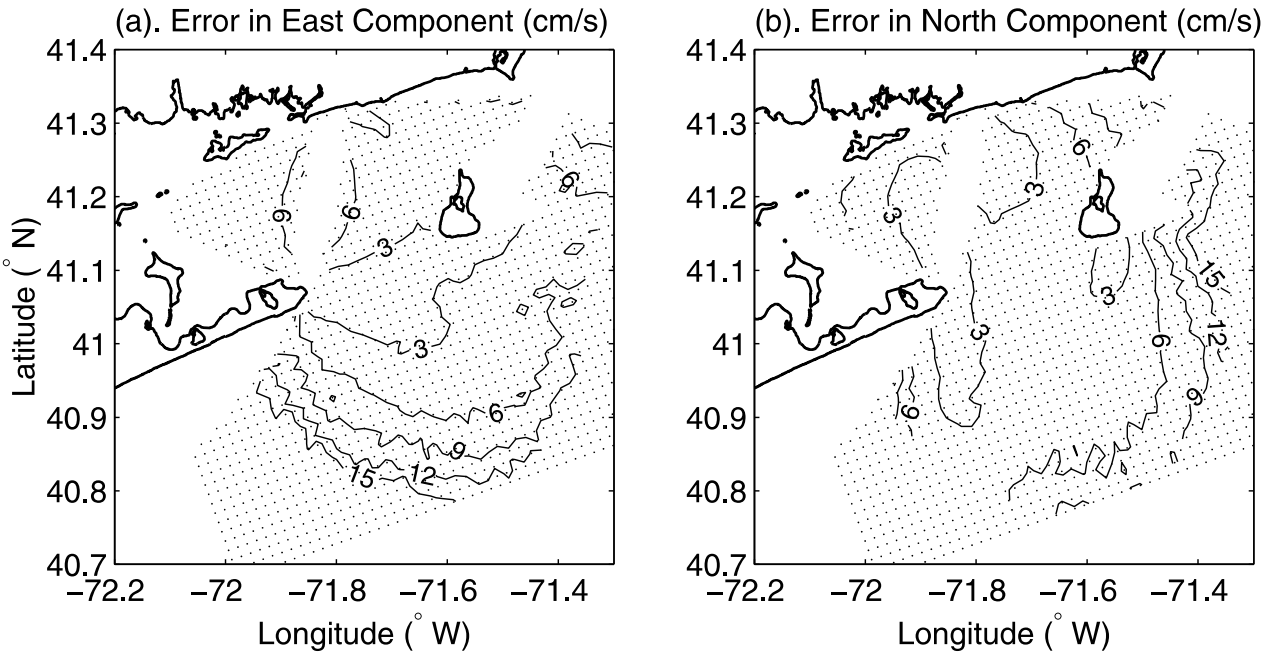

Figure 3. Median standard deviation of the CODAR vector components computed over the period June 2000 to December 2001.

filtering. These data points were subsequently removed from the filtered time series, leaving low-pass current values only at times when vector currents were observed.

[11] The low-passed currents were subsequently averaged over each month to produce monthly averaged Eulerian mean fields. As is shown below, tidal velocities are generally large compared to mean velocities and exhibit locally high spatial variability. In such a case, it is possible that the Eulerian and Lagrangian mean velocities might differ substantially [*Longuet-Higgins*, 1969]. Although the focus of this paper is not Lagrangian trajectories, we have nonetheless carried out particle-tracking experiments to estimate Lagrangian mean velocities. We find that the qualitative picture of the monthly averaged flow is similar in both Eulerian and Lagrangian frameworks. Thus we present only Eulerian currents here, with detailed study of the differences between Eulerian and Lagrangian currents left for future work.

2.2. ADCP Currents

[12] For the 2000–2001 period, six main deployments (Table 1) of an array of bottom-mounted acoustic Doppler current profilers (ADCPs) in the FRONT region (Figure 1) were made. Each deployment involved from one to five instruments for time periods of 1–5 months. Instrument locations varied, primarily due to constraints involving the networked acoustic modems [*Codiga et al.*, 2004] used to maintain real-time communication with the ADCPs. Vertical resolution was nominally 0.5 m (600 kHz units) or 1 m (300 kHz units), and ensemble averaging was nominally over 20 min. The shallowest 2–3 m of the water column are omitted due to acoustic backscatter contamination, and the 2–3 m above the bottom are not sampled. Further details of the ADCP deployments and processing are provided by *Codiga and Houk* [2002]. ADCP currents were low-pass filtered using the same Butterworth filter applied to CODAR currents (section 2.1).

2.3. Hydrographic Data

[13] The seasonal cycle in the hydrographic characteristics of the FRONT region was assessed using historical CTD and bottle casts to supplement the CTD data collected under the FRONT project. FRONT hydrographic surveys

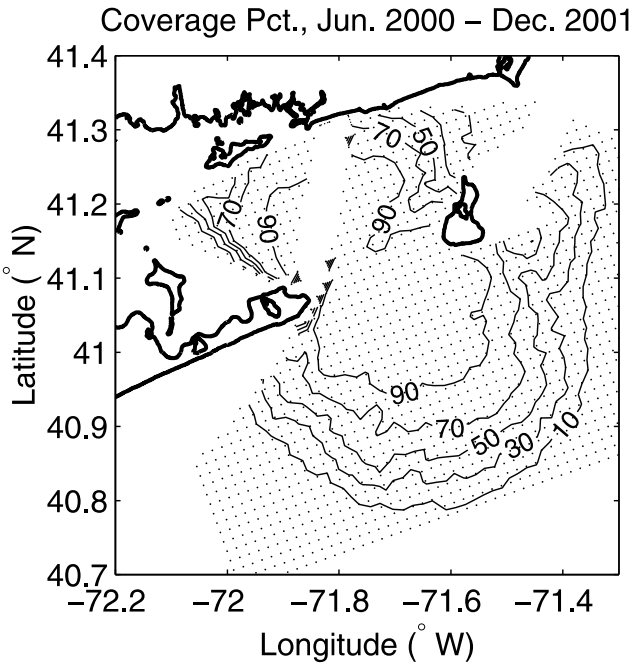

Figure 4. Temporal coverage in percent for CODAR surface current vectors.

Table 1. ADCP Record Start Date, End Date, Mooring Location, and Water Depth

ADCP Record	Start (yyyy/mm/dd)	End (yyyy/mm/dd)	Longitude, °W	Latitude, °N	Depth, m
WI00-S	1999/12/13	2000/02/22	−71.662	40.939	48
WI00-N	1999/12/13	2000/02/23	−71.758	41.026	28
SP00-W	2000/04/28	2000/06/13	−71.767	40.944	46
SP00-E	2000/04/28	2000/06/14	−71.654	41.022	45
FA00-W	2000/10/24	2000/12/09	−71.742	40.986	45
WI01-E	2000/12/19	2001/02/22	−71.684	40.978	42
WI01-W	2000/12/19	2001/02/22	−71.742	40.986	45
SP01-W	2001/03/14	2001/06/03	−71.788	40.980	34
SP01-C	2001/03/14	2001/05/28	−71.711	40.981	47
SP01-E	2001/03/15	2001/06/05	−71.640	40.987	44
SP01-S	2001/03/14	2001/08/23	−71.701	40.954	49
FA01-W	2001/09/05	2002/03/10	−71.788	40.998	33
FA01-E	2001/10/02	2002/03/12	−71.677	41.030	49
FA01-S	2001/10/02	2001/12/11	−71.710	40.973	55
FA01-C	2001/10/07	2002/01/19	−71.732	41.014	37

were performed in May and October 2000 and April, May, September, and November, 2001, and are described further by J. O'Donnell and A. E. Houk, The hydrographic structure of the estuarine outflow from Long Island Sound, manuscript in preparation, 2004. Archived hydrographic profiles for the region were extracted from the 1998 World Ocean Database [*Conkright et al.*, 1998]. The July front probability map from the historical data set described by *Ullman and Cornillon* [1999] (Figure 2a) was used as a guide in defining inshore (zone 1), frontal (zone 2), and offshore (zone 3) zones to assess the cross-frontal hydrographic structure (Figure 5). Zones A and B in Figure 5 were used to define the along-shelf structure. Hydrographic profiles in each of these regions were averaged into 10-m vertical bins and subsequently averaged by month to produce mean profiles of temperature, salinity, and density for each month of the year. Although the profiles in a given month were generally well distributed throughout the regions, the number of profiles entering into the individual monthly averages was highly variable, ranging from approximately 10 to 150, reflecting the fact that FRONT CTD surveys were carried out during spring and fall months only. To verify that the results were not biased by such a sampling problem, we computed a monthly climatology using only the archived data and a 2-month averaged climatology with all hydrographic casts included. The resulting climatologi-

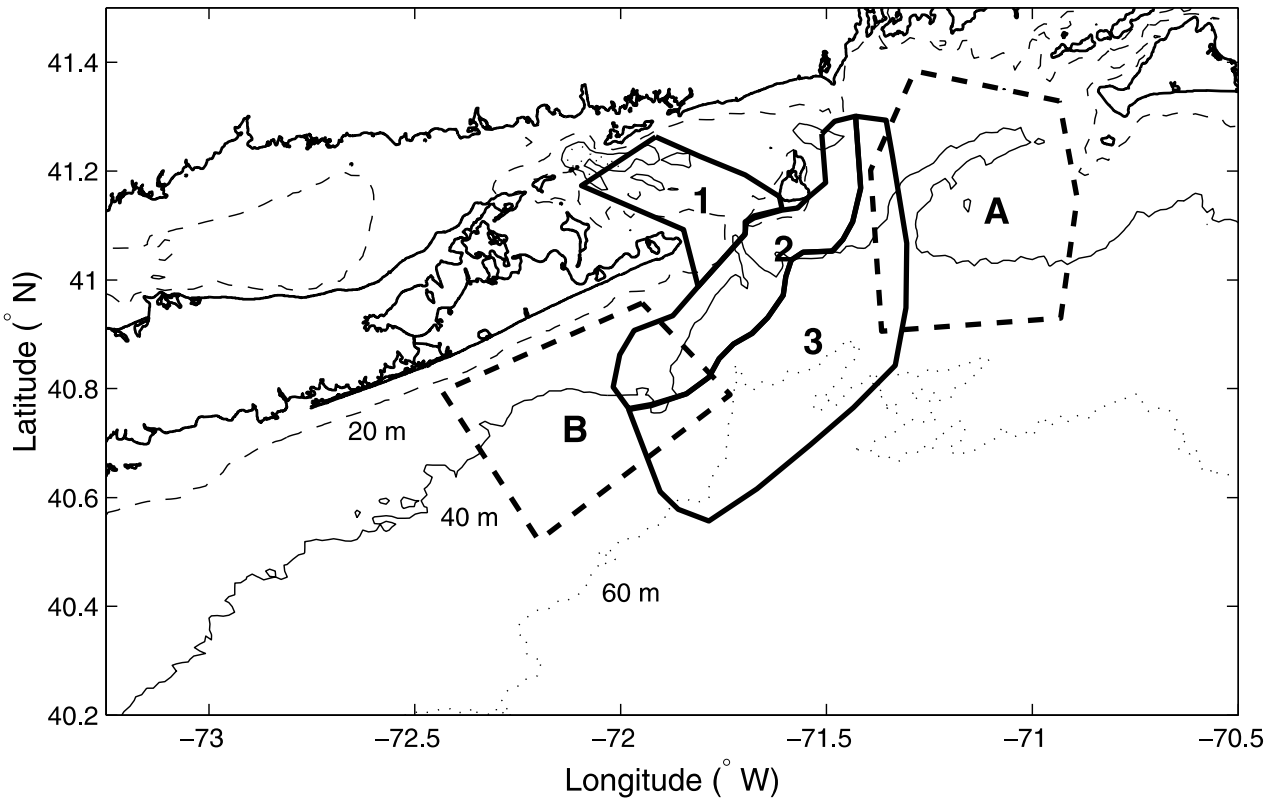

Figure 5. Zones used for averaging the hydrographic observations. Across-shelf and along-shelf density structure is estimated using data from zones 1–3 and zones A and B, respectively.

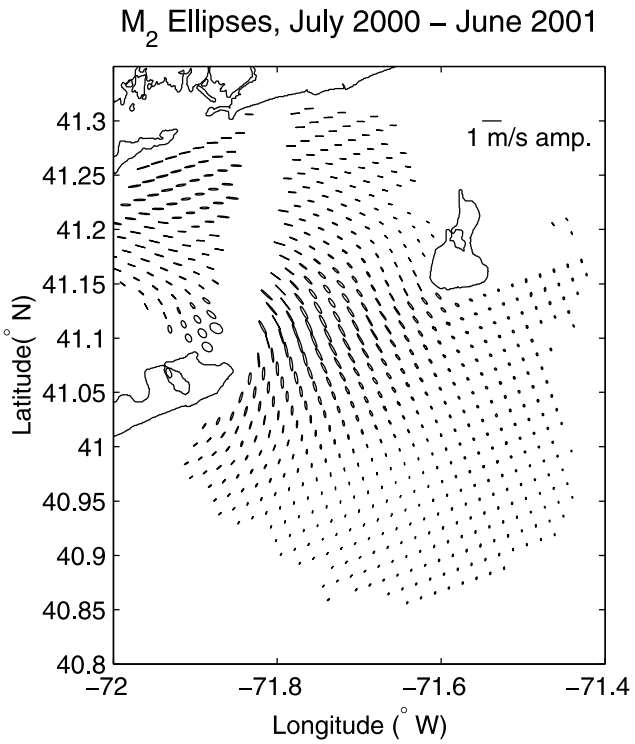

Figure 6. M_2 surface current tidal ellipses derived from 1 year of CODAR observations.

cal hydrographies differed only in minor ways from the 1-month averaged climatology computed using all profiles; thus we present the latter here.

2.4. Sea Level Observations

[14] Hourly water level measurements at New London, Connecticut (Figure 1), for 2000–2001 were obtained from the National Ocean Service (http://co-ops.nos.noaa.gov). After low-pass filtering with the 36-hour Butterworth filter, the inverse barometer effect was removed using atmospheric pressure observations from a nearby National Weather Service station (Groton Airport). The resulting time series was subsequently averaged by month to form a mean monthly adjusted sea level record.

3. Results

3.1. Surface Circulation Field

[15] Tidal currents in the Long Island Sound outflow region are strong, with M_2 surface current amplitudes reaching 0.8 m/s in the vicinity of Montauk Point (Figure 6). Amplitudes decrease rapidly just inshore of the ADCP mooring zone, becoming low (0.1–0.15 m/s) in the southern part of the coverage area. This rapid spatial variability appears to give rise to large tidally rectified flows in the immediate vicinity of Montauk Point (C. A. Edwards et al., Spring-summer frontogenesis at the mouth of Block Island Sound: 1. A numerical investigation into tidal and buoyancy-forced motion, submitted to *Journal of Geophysical Research*, 2004). The CODAR currents are used to estimate this forcing in the mooring zone (section 3.4) where, in contrast to inshore areas, it is found to be weak compared to other terms in the momentum balance.

[16] The low-pass filtered CODAR currents were averaged over the entire 19-month record to provide a mean surface current field (Figure 7a). Strong outflow from Long Island Sound is observed in the northwest part of the region with speeds of up to 0.25 m/s. The outflow appears to be convergent in the vicinity of the Montauk-Misquamicut baseline; however, the increase in east component errors in this region (see Figure 3a) and the lack of vectors on the baseline make interpretation difficult. East of the baseline, there is evidence that the outflow splits, with part flowing south around Montauk Point and part continuing east and retroflecting near Block Island. The most striking feature of the mean current field is, however, the strong (0.15–0.2 m/s) jet flowing southwest from the vicinity of Block Island. This feature is spatially coincident with the region of high summer front probability (Figure 2a). Although the jet strengthens south of Montauk Point where the Long Island Sound outflow joins it, it appears that a substantial part of the flow originates upshelf to the northeast.

[17] Principal axes of the monthly current variability, also computed over the whole record (Figure 7b), show that fluctuations are strongly anisotropic in both the outflow and jet regions. Observed major axis amplitudes of ~0.1 m/s in both the outflow and jet regions indicate substantial variability relative to the mean field. Major axes in these areas are roughly aligned with mean flow directions, although in the jet, there is a small clockwise rotation of the former such that the dominant variability occurs more in the east-west direction, whereas the mean flow is roughly southwestward. Averaging over the frontal region (zone 2 in Figure 5), the mean major axis orientation is toward 57.5°T. In the remainder of the paper, the along-shelf or along-front (x) coordinate is oriented in this direction, with the cross-shelf or cross-front (y) direction orthogonal to this, or roughly shoreward.

3.2. Seasonal Variability in Frontal Zone Current

[18] The southwestward jet evident in the mean surface current map (Figure 7a) exhibits substantial variability on seasonal timescales. It is strongest in summer, with monthly mean surface currents of ~0.25 m/s observed in its core (Figure 8b). The jet is typically absent in winter, as seen in the monthly mean current map from December 2000 (Figure 8a). At this time, the current pattern is dominated by the outflow from Long Island Sound with no evidence of flow into the region from the northeast. There is no indication in the winter map of an offshore shift or spatial smearing of the jet corresponding to the offshore shift and increased width of the high frontal probability band in Figure 2b. It is noteworthy that similar seasonal variability in along-shelf flow has been recently observed by *Kincaid et al.* [2003] south of Narragansett Bay (located to the northeast of the FRONT region).

[19] The monthly CODAR surface currents were resolved into along-shelf (u) and across-shelf (v) components, and these were subsequently averaged spatially over the frontal region to provide a measure of the mean along-shelf and cross-shelf currents for each month. This has also been performed for the monthly ADCP near-surface (4–6 m) and near-bottom (34–36 m) currents for those current profilers located within the frontal zone. Note that some ADCP

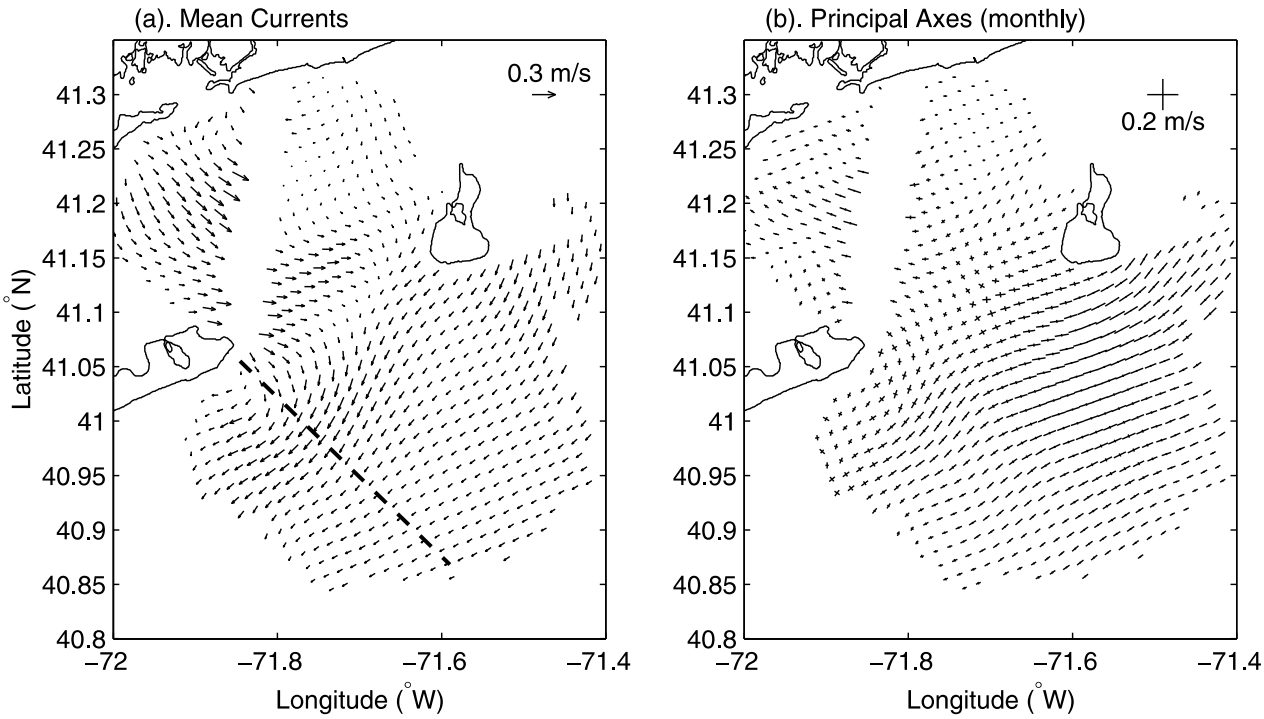

Figure 7. (a) Mean CODAR surface currents and (b) principal axes of the monthly current variance for the period June 2000 to December 2001. The dashed line in Figure 7a defines the transect across which the transport is subsequently computed.

locations were at depths <35 m; for these instruments, only near-surface estimates were made. For the following analysis, only those ADCP monthly means with observations spanning at least 10 days were retained.

[20] A clear seasonal cycle is evident in the time series of monthly mean CODAR and ADCP surface and bottom along-shelf currents, with near-surface current values approximately zero in November-February and peak values of

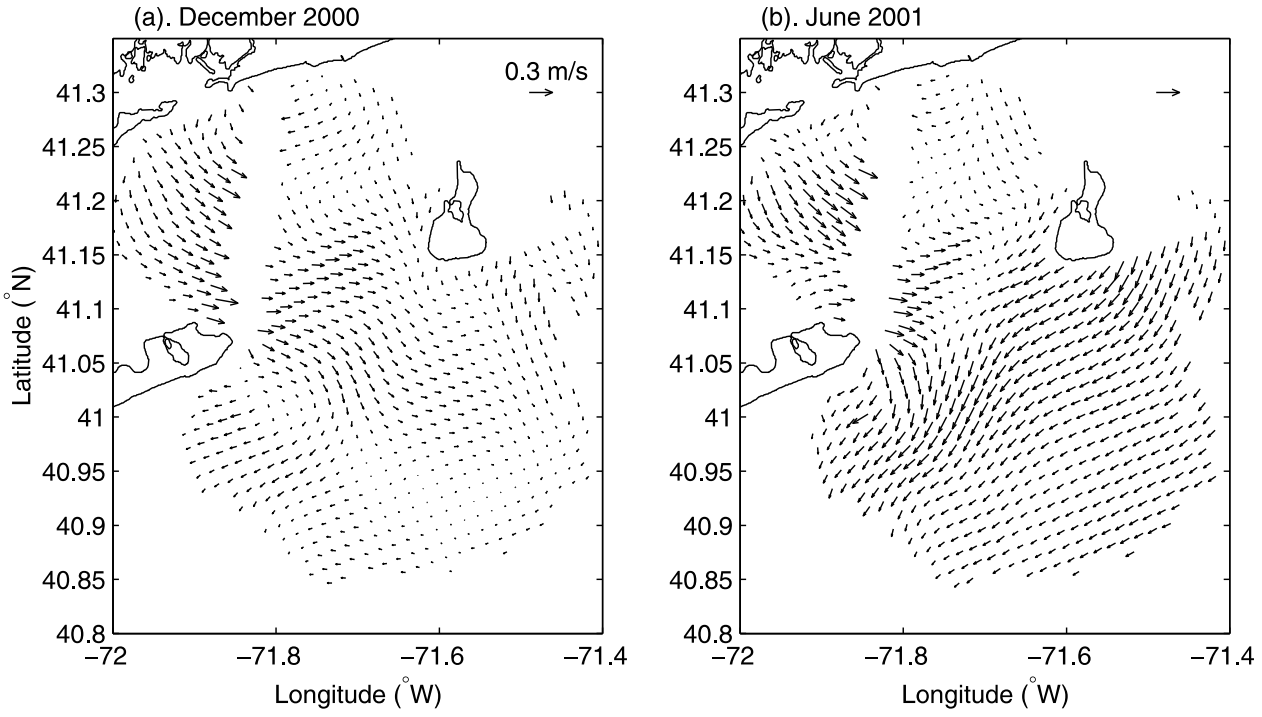

Figure 8. Monthly mean low-pass CODAR surface currents during (a) December 2000 and (b) June 2001.

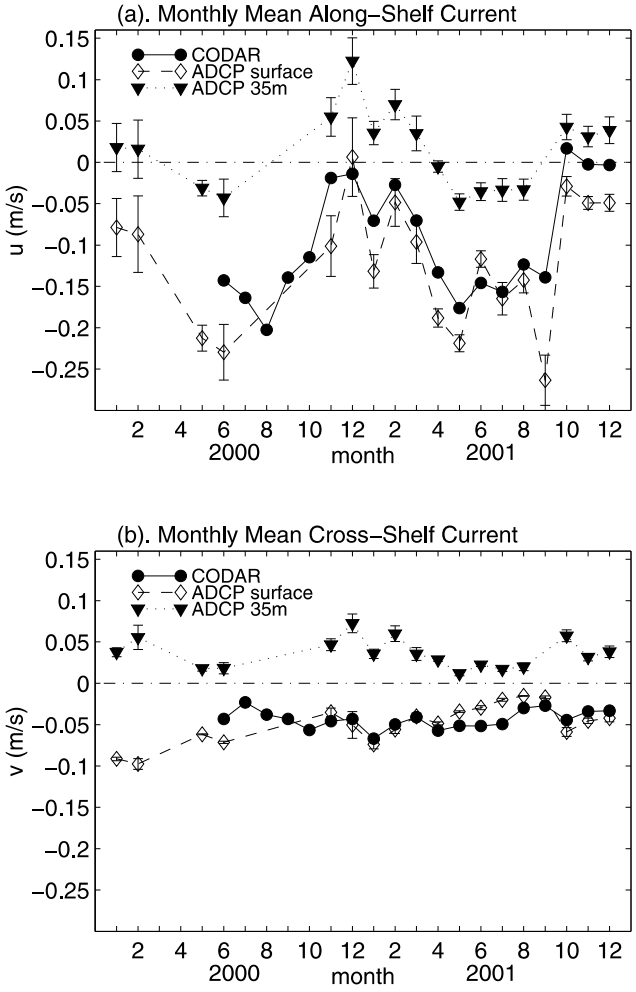

Figure 9. Mean (a) along-shelf and (b) across-shelf current, averaged over the frontal zone (zone 2) defined in Figure 5 and over individual months for both CODAR and ADCP near-surface (4–6 m) and near-bottom (34–36 m) velocities. The along-shelf direction is positive toward 57.5°T.

−0.15 to −0.25 m/s (directed roughly southwestward) occurring in May–September (Figure 9a). Near-bottom currents vary similarly with small negative values in summer and slight (0.05–0.1 m/s) positive values in winter. The vertical shear (not shown) is approximately constant to within the estimated errors, with a mean value of ∼0.14 m/s over 30 m.

[21] Currents in the cross-shelf direction are generally weaker O(0.05 m/s) than their along-shelf counterparts, with surface currents directed offshore and near-bottom currents directed onshore (Figure 9b). There is little evidence of a seasonal signal in the across-shore CODAR or ADCP surface currents. The near-bottom current, however, appears to vary seasonally with slightly stronger onshore flow during the winter months (Figure 9b), as would be consistent with the cross-shelf circulation associated with stronger offshore and upshelf-directed wind stress that occurs in winter in this region (see below).

3.3. Regional Hydrography

[22] To set the stage for the discussion of the depth averaged momentum balance in section 3.4, in which the cross-shore baroclinic pressure gradient is an important term, the regional hydrography is examined next. Within the zones defined in Figure 5, all historical CTD and bottle casts, in addition to CTD casts from FRONT surveys, were monthly averaged within 10-m vertical bins to produce a regionally averaged seasonal depth-time series. In this section we discuss the hydrography only in the cross-shelf zones, although both along-shelf and cross-shelf hydrographic gradients are assessed in section 3.4.

[23] The region inshore of the frontal zone (zone 1) is nearly well mixed all year with respect to temperature, with salinity stratification strongest in spring to summer and weak in winter (Figure 10). The resulting density field exhibits moderate vertical stratification peaking in late summer. In the offshore region (zone 3), salinity is much less variable, suggesting that the frontal region represents the outer boundary of estuarine influence on the shelf. Here density is most strongly controlled by temperature with lightest surface waters (and most intense vertical stratification) occurring in middle to late summer.

[24] The relative phasing of the hydrographic variability discussed above brings about a surprising variability in the cross-shore density difference. The density difference is typically positive, corresponding to denser offshore waters, becoming weak near the surface in summer because of higher near-surface temperatures in the offshore region, likely due to reduced vertical mixing there (Figure 11a). Peak density differences occur near surface in early spring and near bottom during the summer/early fall period. The early spring peak results from a salinity decrease in the inshore zone, presumably due to outflow from the estuary, while the summer, near-bottom increase arises from the relatively high near-bottom temperatures resulting from stronger vertical mixing occurring within Block Island Sound (Figures 11b and 11c). The depth-averaged cross-frontal density difference (Figure 11d) is dominated by the salinity effect in the mean, with the effect of temperature producing an increase during summer.

3.4. Depth-Averaged Momentum Balance

[25] An evaluation of the terms in the momentum balance can provide an understanding of the seasonal variability that we observe in the southwestward jet. The depth and tidally averaged momentum balances in the x (along-shore) and y (cross-shore) directions are

$$\frac{\partial \bar{u}}{\partial t} - f\bar{v} = -\frac{1}{\rho_0 H}\int_{-H}^{0}\frac{\partial P}{\partial x}\,dz + \frac{\tau_{sx}}{H} - \frac{\tau_{bx}}{H} - \langle \bar{U}\frac{\partial \bar{U}}{\partial x} + \bar{V}\frac{\partial \bar{U}}{\partial y}\rangle \tag{1}$$

$$\frac{\partial \bar{v}}{\partial t} + f\bar{u} = -\frac{1}{\rho_0 H}\int_{-H}^{0}\frac{\partial P}{\partial y}\,dz + \frac{\tau_{sy}}{H} - \frac{\tau_{by}}{H} - \langle \bar{U}\frac{\partial \bar{V}}{\partial x} + \bar{V}\frac{\partial \bar{V}}{\partial y}\rangle, \tag{2}$$

where (U, V) and (u, v) are, respectively, tidal and tidally averaged velocities in the x and y directions, P is pressure, τ_s and τ_b are surface and bottom stresses, H is the water depth, the overbars denote a depth-averaged quantity, and $\langle\rangle$ represents a tidal average. The last two terms on the right-hand side of equations (1) and (2) are the advective tidal stresses [*Visser et al.*, 1990], which are

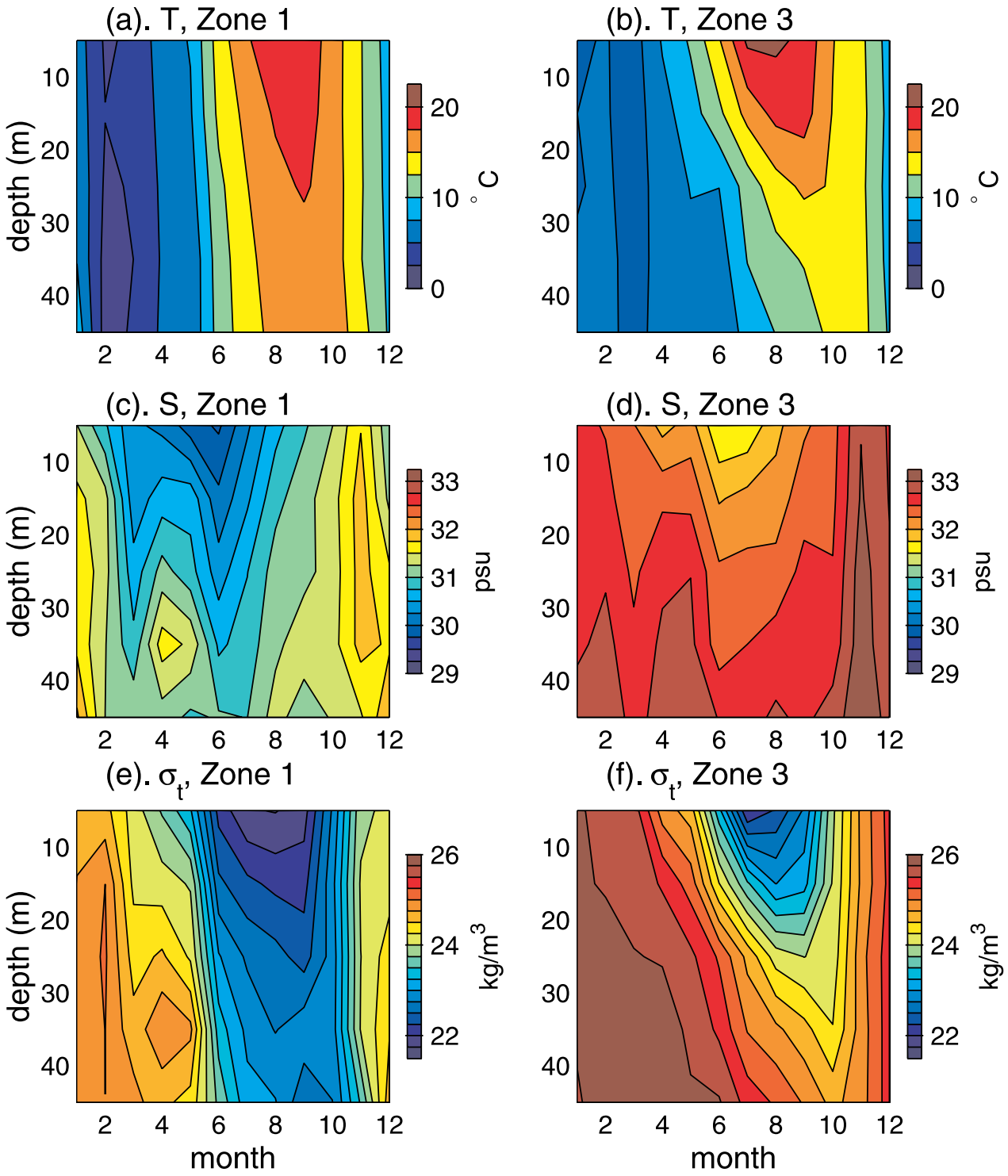

Figure 10. Seasonal cycle in (a, b) temperature, (c, d) salinity, and (e, f) σ_t for the zones inshore (zone 1) and offshore (zone 3) of the frontal zone. Hydrographic profiles taken within each of these zones were averaged with respect to month in 10-m vertical bins.

responsible for the transfer of energy from tidal period motions to the mean flow. The nonlinear advection terms involving $\bar{u}$ and $\bar{v}$ have been neglected in equations (1) and (2) based on the observation that $U, V > \bar{u}, \bar{v}$. In equations (1) and (2), ρ_0 is a reference density relating the dimensionless density anomaly to the actual density [*Csanady*, 1979]

$$\rho = \rho_0[1 + \epsilon(x, y, z, t)]. \tag{3}$$

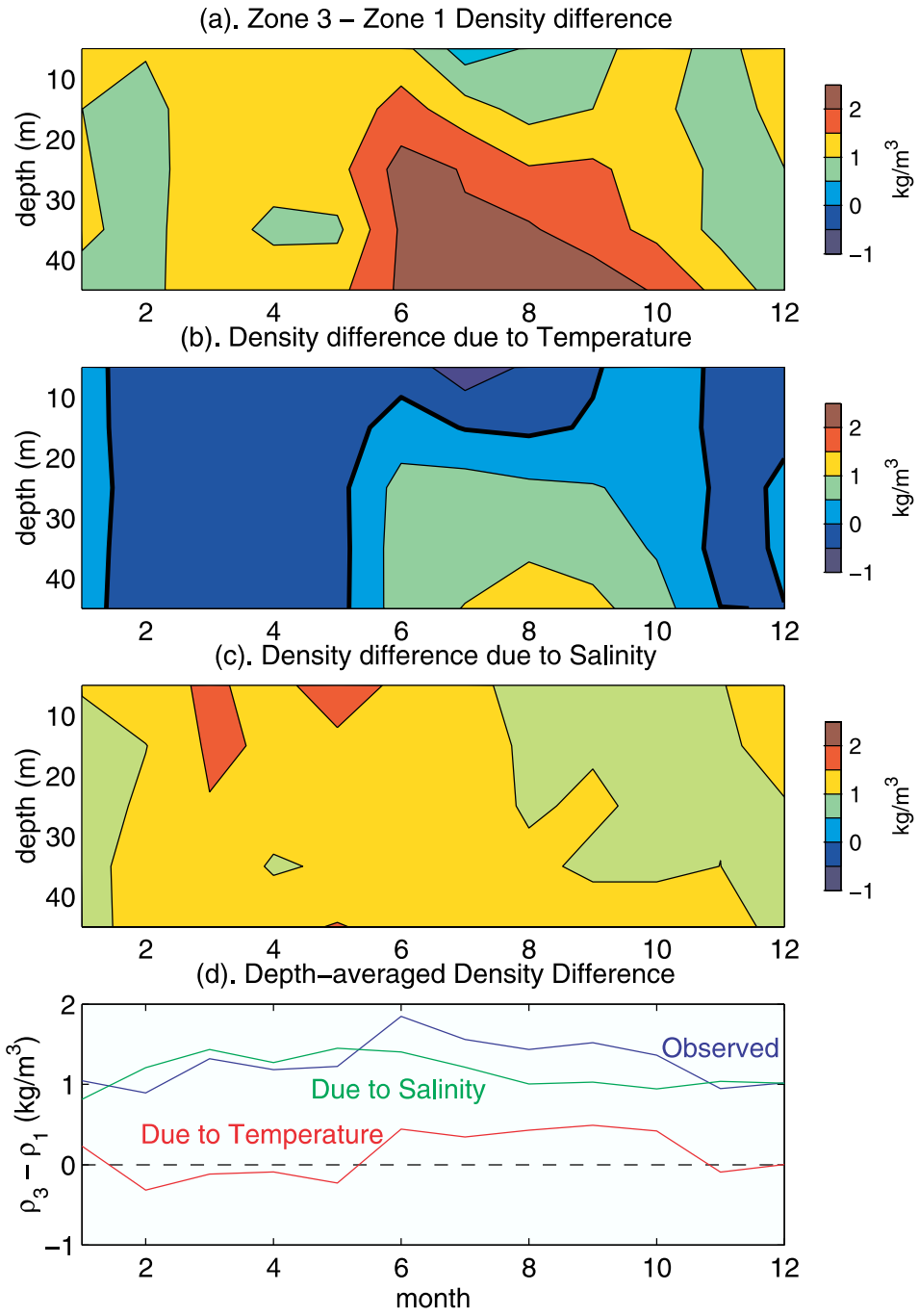

Figure 11. Seasonal cycle in (a) density difference between offshore and inshore zones, (b) density difference due to temperature differences, (c) density difference due to salinity differences, and (d) depth-averaged density difference.

With ρ_0 chosen to be the maximum observed density (at depth in zone 3), $\epsilon < 0$.

[26] We now examine the pressure gradient term more closely, starting with the term prior to vertical averaging. Following *Csanady* [1979], a typical horizontal pressure gradient at depth z is written as

$$\frac{1}{\rho_0}\frac{\partial P}{\partial y} = g\frac{\partial \eta}{\partial y} + g\frac{\partial}{\partial y}\int_z^0 \epsilon\, dz'. \tag{4}$$

If we define the surface steric height relative to a reference level H_m as:

$$\eta_s = -\int_{-H_m}^0 \epsilon\, dz', \tag{5}$$

then

$$g\frac{\partial \eta_s}{\partial y} + g\frac{\partial}{\partial y}\int_{-H_m}^0 \epsilon\, dz' = 0. \tag{6}$$

Subtracting equation (6) from the right-hand side of equation (4) and combining the integrals gives

$$\frac{1}{\rho_0}\frac{\partial P}{\partial y} = g\frac{\partial \eta_{ns}}{\partial y} - g\frac{\partial}{\partial y}\int_{-H_m}^{z} \epsilon\, dz', \tag{7}$$

where $\eta_{ns} = \eta - \eta_s$ is the surface departure from the steric setup level. The first term is thus the pressure gradient arising from non-steric sources. The second term represents the gradient of the pressure surface at depth z relative to the reference level and is non-zero only in the presence of sloping isopycnals. Referencing the pressure to a deep level as in equation (7) therefore allows the pressure gradient to be partitioned into non-steric and steric parts, which is not the case in equation (4) where the first term potentially contains contributions from both sources. Depth averaging equation (7), applying Leibnitz's rule, and simplifying the resulting double integral using integration by parts [*Csanady*, 1979] results in

$$\frac{1}{\rho_0 H}\int_{-H}^{0}\frac{\partial P}{\partial y}\,dz' = g\frac{\partial \eta_{ns}}{\partial y} + \frac{g}{H}\frac{\partial}{\partial y}\int_{-H}^{0}\epsilon z'\,dz' - g\frac{\partial}{\partial y}\int_{-H_m}^{-H}\epsilon\,dz'. \tag{8}$$

[27] The baroclinic gradient terms in equation (8) will be evaluated by differencing integrals evaluated in regions 1 and 3 (Figure 5) from the hydrography. We take $H_m = 50$ m, the approximate depth in region 3. Although depths in this range occur there, region 1 is separated from regions 2 and 3 by a sill (depth ~35 m), implying that the deep hydrography in region 1 will not impact the dynamics in the area of interest (region 2). The integrals in equation (8) are thus evaluated only for the upper 35 m in region 1. The third term on the right-hand side is evaluated as by *Csanady* [1979] by integrating along the bottom from $-H_M$ to $-H$. The corresponding along-shore gradients are estimated from the averaged hydrography in zones A and B (Figure 5).

[28] Over the seasonal timescales of interest here, the local accelerations in equations (1) and (2) can be safely neglected. With this approximation, substituting equation (8) and the corresponding expression for the along-shore gradient into equations (1) and (2) and moving all terms to the right-hand side gives the steady, depth-averaged momentum balances

$$0 = f\bar{v} - g\frac{\partial \eta_{ns}}{\partial x} + BC_x + \frac{\tau_{sx}}{H} - \frac{\tau_{bx}}{H} - T_x \tag{9}$$

$$0 = -f\bar{u} - g\frac{\partial \eta_{ns}}{\partial y} + BC_y + \frac{\tau_{sy}}{H} - \frac{\tau_{by}}{H} - T_y, \tag{10}$$

where T_x and T_y are the tidal stress terms, and the depth averaged baroclinic terms BC_x and BC_y are given by

$$BC_x = -\frac{g}{H}\frac{\partial}{\partial x}\int_{-H}^{0}\epsilon z'\,dz' + g\frac{\partial}{\partial x}\int_{-H_m}^{-H}\epsilon\,dz' \tag{11}$$

$$BC_y = -\frac{g}{H}\frac{\partial}{\partial y}\int_{-H}^{0}\epsilon z'\,dz' + g\frac{\partial}{\partial y}\int_{-H_m}^{-H}\epsilon\,dz'. \tag{12}$$

Except for the second terms on the right-hand sides, which are the non-steric components of the pressure gradient force, all terms in equations (9) and (10) can be estimated from the data. Assuming the validity of equations (9) and (10), we then infer the values of the former, due to the barotropic pressure gradient arising from non-steric effects.

[29] The Coriolis and bottom stress terms are evaluated at each available ADCP mooring, averaging over each month and then spatially over the frontal zone as described in section 3.2. Bottom stress is computed using a quadratic law applied to the unfiltered near-bottom velocity and is subsequently low-pass filtered and averaged as for the currents. The drag coefficient at a height appropriate to the near-bottom velocity was adjusted from the 1 m value of 2.5×10^{-3} assuming a logarithmic layer. Wind stress at buoy 44025 was computed using the instantaneous wind and the neutral drag coefficient formulation of *Large and Pond* [1981], with the stress also low-pass filtered and monthly averaged. The baroclinic terms are evaluated on a mean-monthly basis using the archived hydrography and the FRONT CTD data as described above. The mean seasonal cycle in baroclinic forcing is assumed to apply to each of the 2 years considered. The tidal stress terms are evaluated at each CODAR grid point using M_2 tidal currents derived from harmonic analysis of CODAR currents (see Figure 6) and are subsequently averaged spatially over the ADCP mooring area. The use of surface rather than depth-averaged currents in this calculation likely results in a slight overestimate of the tidal stresses because of the reduction in tidal current amplitude with depth [*Codiga and Rear*, 2004]. Computed tidal stresses are treated as temporally constant based on the neglect of interactions with other semidiurnal constituents.

[30] Time series of the terms in equations (9) and (10) for the 2-year period are shown in Figure 12. The across-shore balance (Figure 12b) is predominantly geostrophic, with the baroclinic and (inferred) non-steric barotropic pressure gradient components both significant. The tidal stress is lower in magnitude, although it is significantly different from zero and of the proper sign to balance part of the mean southwestward (along-shore) flow. Frictional stresses are negligible in the across-shore direction. The baroclinic pressure gradient term is negative (offshore) throughout the year, corresponding to an upward slope of pressure surfaces (relative to the pressure at the reference depth) onshore due to the presence of less dense water nearshore. The seasonal variability in depth-averaged baroclinic forcing is of the proper sign and phase to explain a portion of the variability in the depth-averaged along-shelf flow. However, a substantial cross-shore non-steric barotropic gradient is needed to close the momentum balance. The inferred non-steric barotropic pressure gradient term is near zero in summer and peaks in winter with values of O(1×10^{-5} m/s^2) corresponding to a surface sloping down toward the coast.

[31] Except for the stresses, the terms in the along-shore momentum balance (Figure 12a) are roughly an order of magnitude smaller than the corresponding terms in the across-shore balance and exhibit no obvious seasonal variability. The Coriolis acceleration and the inferred non-steric barotropic pressure gradient term are on average the largest of the terms we can estimate, although the uncertainties are

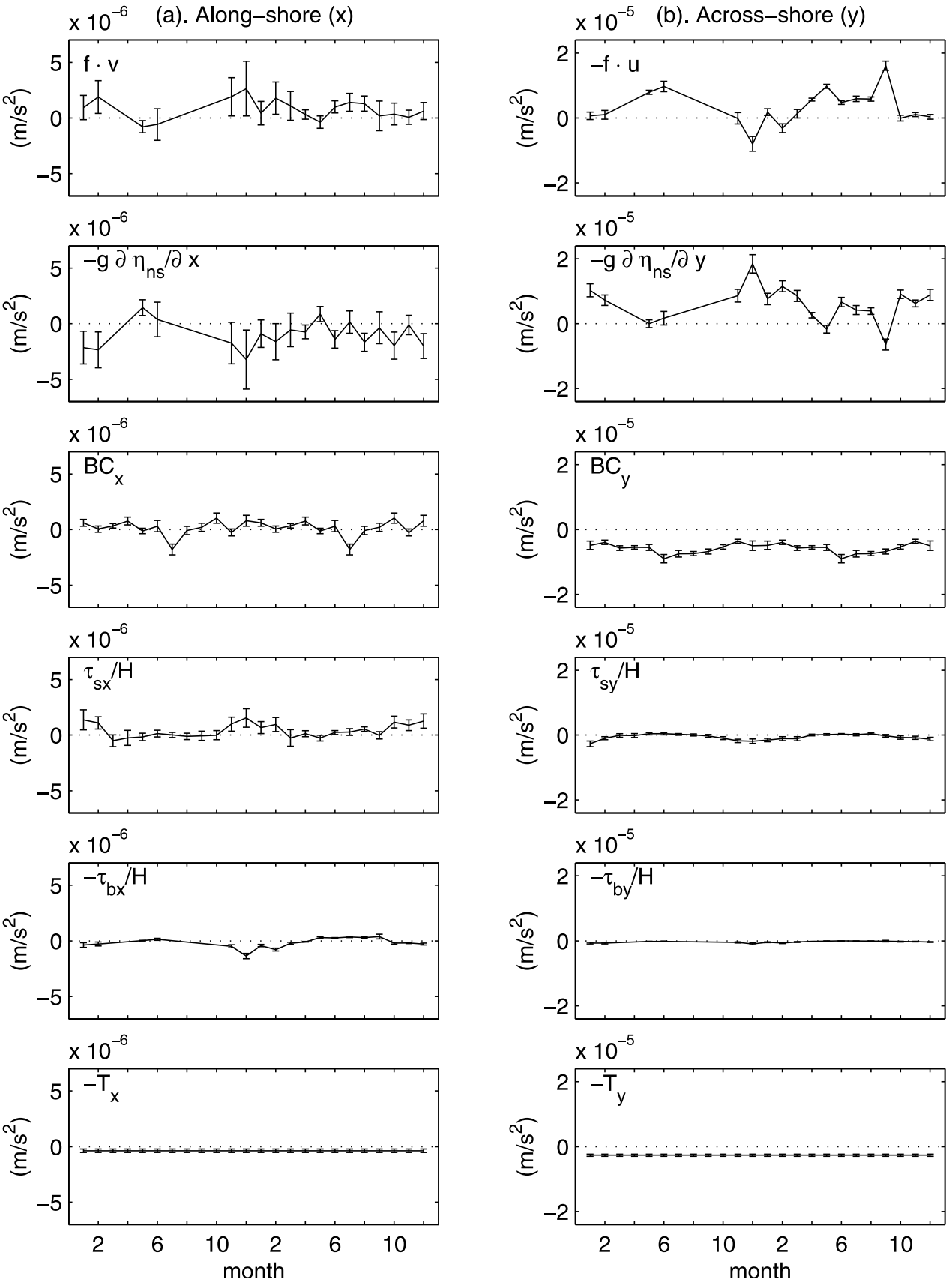
(a). Along–shore (x)
(b). Across–shore (y)
x 10^−6
x 10^−5
f · v
−f · u
−g ∂ η_ns/∂ x
−g ∂ η_ns/∂ y
BC_x
BC_y
τ_sx/H
τ_sy/H
−τ_bx/H
−τ_by/H
−T_x
−T_y
(m/s^2)
month
2 6 10 2 6 10

Figure 12

often as large as the estimated values. The mean non-steric barotropic term is negative, corresponding to an upward slope of the sea surface in the positive x direction. A seasonal cycle is evident in the along-shore wind stress and bottom stress. Wind stress is upshelf during the winter months and approximately balances the downshelf-directed bottom stress during this period. In summer, wind stress is weak, with typical monthly mean values not significantly different from zero. Bottom stress is also weak in summer, as expected from the observation of low near-bottom velocities at this time (see Figure 9). The estimated along-shore baroclinic gradient is quite small, as is the tidal stress term.

4. Discussion

[32] The conclusion of *Beardsley et al.* [1985] that the along-shelf transport over the shelf and slope of the Middle Atlantic Bight does not vary seasonally has been the generally accepted view in this region. The observations reported here of the southwestward jet in the Long Island Sound outflow region and recent results of *Kincaid et al.* [2003] provide a contrasting view for the inner shelf. It is useful therefore to estimate the transport associated with the jet in order to compare it with the transport computed by *Beardsley et al.* [1985]. We estimate the transport perpendicular to the line extending approximately southeastward from Montauk Point (shown in Figure 7a). The horizontal spatial structure is provided by the CODAR velocity fields and the vertical structure by the ADCP shear in Figure 9 with a value of 4.7×10^{-3} s^{-1}. Because this shear value is derived from observations within the frontal zone, it is not applied uniformly over the section. In the deeper region offshore of the jet, we use a shear value that produces zero velocity at the bottom. The transport associated with the mean jet in Figure 7a, estimated with these assumptions, is 5×10^4 m^3/s or 0.05 Sv. For the intensified jet in summer (Figure 8b), we get 0.07 Sv. The mean value is 10–15% of the *Beardsley et al.* [1985] value of 0.38 Sv south of Nantucket Shoals.

[33] The handling of the depth-averaged pressure gradient in section 3.4 differs from the standard coastal oceanographic method typified by *Csanady* [1979] and thus merits discussion. The formulation provided here explicitly separates steric and non-steric contributions, allowing isolation of the buoyancy-driven component of the depth-averaged flow. This is accomplished through use of a reference level at depth instead of the surface as is more customary [*Csanady*, 1979]. If we were to compute the standard depth-averaged baroclinic pressure gradient referenced to the surface, the buoyancy-driven component u_b would be an upshelf flow opposing a stronger downshelf motion in geostrophic balance with the barotropic component of the pressure gradient resulting from cross-shore surface slopes arising from both steric and non-steric effects. In other words, in this case the baroclinic component would have represented a correction (reduction), due to thermal wind shear, to the depth averaged barotropic flow.

[34] The analysis of the depth-averaged momentum balance in the FRONT region suggests that the seasonality observed in the monthly averaged currents arises from variability in both the baroclinic and barotropic components of the depth-averaged across-shelf pressure gradient. The depth-averaged density contrast between waters inshore of the frontal zone and waters offshore reaches a maximum in summer due to both the influx of riverine runoff to the inshore zone and non-uniform vertical redistribution of surface heat flux. Although the surface heat fluxes on the inshore and offshore sides of the jet are likely to be roughly equal, the preferential vertical redistribution of this heat in the inshore zone due to tidal mixing produces an important component of the depth-averaged baroclinic pressure gradient because this gradient in equation (12) is weighted more heavily by densities from deeper levels.

[35] The weakening of the southwestward jet in winter is associated with the development of an onshore-directed barotropic pressure gradient force associated with the slope of the surface relative to the steric height (see equation (7)). This gradient may arise from the effects of local wind stress or possibly from upshelf sources. If we assume that the wind-driven surface elevation goes to zero at some distance from shore, the magnitude of the gradient inferred in section 3.4 can be checked using coastal sea level data combined with the hydrographic observations as follows.

[36] The mean monthly time series of adjusted sea level exhibits a maximum in September and a minimum in February (Figure 13a). The monthly mean steric height in zone 1 computed using equation (5) is observed to undergo a similar annual cycle (Figure 13b). Subtracting the steric height from the adjusted sea level provides an estimate of the monthly sea level deviations from the steric height field (Figure 13c). The relative height is negative during the winter months and near-zero in summer with positive values occurring in spring and late fall. Using the winter values of O(−0.05 m) and assuming an offshore length scale for wind-induced surface perturbations of 100 km (roughly the shelf width) gives an onshore barotropic pressure gradient of O(0.5×10^{-5} m/s^2), or approximately half the magnitude of the winter pressure gradients estimated from the momentum balance. This is not entirely unexpected given that the analysis of the momentum balance was carried out over the inner shelf where, due to the exponential structure of the theoretical surface elevation in response to longshore winds [*Csanady*, 1982], the surface slope is larger than the value calculated by differencing coastal and offshore values as we have done. It thus appears that the diagnosed across-shelf pressure gradients are reasonable.

[37] The barotropic pressure gradient variability could result from geostrophic adjustment to large-scale variations in downshelf flow. The lack of a significant annual cycle in transport over the middle and outer shelf (40–120 m depth) south of Nantucket Shoals [*Beardsley et al.*, 1985] suggests

Figure 12. Terms in the depth-averaged momentum balance in the (a) along-shore direction (positive toward 57.5°T) and (b) across-shore direction (positive onshore). From top to bottom the terms are Coriolis, barotropic pressure gradient, baroclinic pressure gradient, wind stress, bottom stress, and tidal stress. The barotropic pressure gradient is inferred as the residual of the computed terms. The error bars represent 1 standard error.

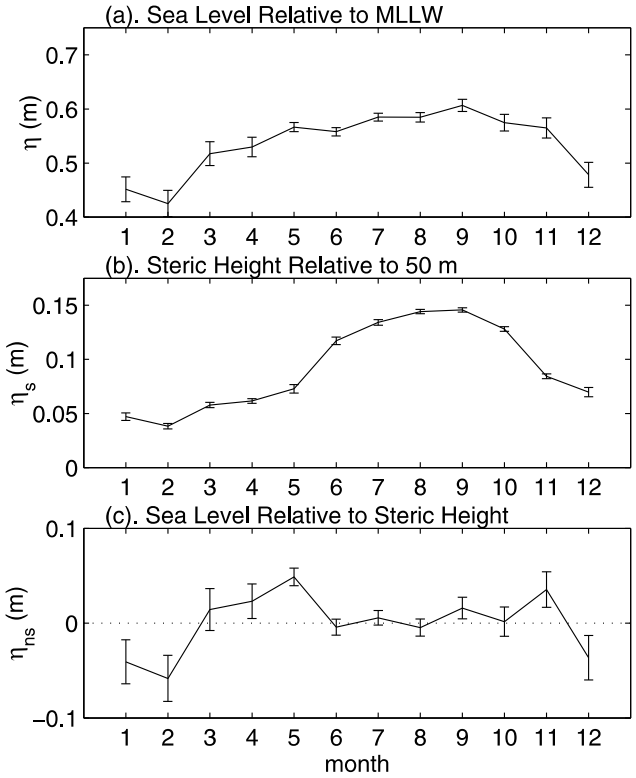

Figure 13. (a) Mean monthly adjusted sea level relative to mean lower low water (MLLW) for New London. (b) Zone 1 mean monthly steric height relative to 50 m. (c). Adjusted sea level relative to steric height. The mean values of the adjusted sea level and steric height curves were subtracted prior to differencing.

that this is not the case. It is possible that the along-shore flow inshore of the 40-m isobath in this area, a region not measured by *Beardsley et al.* [1985], does vary seasonally. The development of an onshore pressure gradient in winter is consistent with the response to wind. Monthly mean wind stress in winter is upshelf (Figure 12) and the divergence of offshore Ekman transport would result in sea level set-down at the coast and a resulting surface sloping downward onshore. While we do not observe seasonal variability in the surface cross-shelf velocity, stronger onshore velocities at depth occur in winter, consistent with deep return flow in response to offshore surface transport.

[38] The weakening of the along-shelf flow over the southern New England inner shelf in winter may be related to the wintertime cross-isobath flow on the southwest side of Nantucket Shoals that was inferred by *Ullman and Cornillon* [2001] from SST observations. The wind stress in winter in that area, as at buoy 44025 from this study, is directed toward the southeast. It is thus upwelling favorable over the southern New England shelf and downwelling favorable over the shelf north of the Shoals where the coast is oriented roughly north-south. In the FRONT region on the southern New England coast, the wind stress acts, through the development of a cross-shore non-steric pressure gradient, to oppose the buoyancy-driven flow. North of Nantucket Shoals, however, the downwelling-favorable wind stress would act to augment the downshelf flow. Thus, assuming roughly equal buoyancy driven flows on either side of the shoals, we can postulate the existence of a zone of convergence of along-shore flow during winter in the Nantucket Shoals region that must be balanced by a divergence in cross-shelf flow. The observations, in winter, of plumes of cold water extending southwest across isobaths from the Shoals by *Ullman and Cornillon* [2001] is consistent with this scenario.

5. Summary and Conclusions

[39] A coastal current jet detected in HF radar and ADCP measurements on the southern New England shelf south of Block Island Sound was found to exhibit strong annual variability. The surface-intensified jet is strongest in summer when the flow is southwestward, with transport of ~0.07 Sv or about 18% of the transport south of Nantucket Shoals, and is essentially absent in winter. The observed seasonal variability on a portion of the inner shelf influenced by local estuarine outflows suggests that the paradigm of seasonally constant alongshelf transport in the Middle Atlantic Bight put forth by *Beardsley et al.* [1985] should be re-evaluated, at least over the inner shelf.

[40] Analysis of the depth-averaged momentum balance indicates that the along-shelf flow is in approximate geostrophic balance. The buoyancy-driven flow, due to the presence of less dense water inshore, is downshelf (southwestward) throughout the year, with some intensification in summer. The weakening of the jet in winter is associated with the intensification of an onshore pressure gradient force arising from non-steric sources. This pressure gradient is consistent with the response to upwelling-favorable wind stress, which increases during winter along this coast. The seasonal variability in the coastal jet is thus due to the combined effects of the annual variability in buoyancy-driven and wind-driven forcing. It is hypothesized that cross-isobath flows observed southwest of Nantucket Shoals may result from an along-shore convergence in wind-driven flow arising from the abrupt coastline bend there.

[41] **Acknowledgments.** Funding from the National Oceanographic Partnership Program through Office of Naval Research grants N00014-99-1-1020 and N00014-99-1-1021 is gratefully acknowledged. The FRONT CTD data were collected and made available by Jim O'Donnell. We are indebted to Todd Fake, Jim Fontaine, and Adam Houk for their assistance on many aspects of the FRONT project. The project benefited greatly from the skills of Captain Turner Cabaniss, mate Dan Nelson, and the crew of the RV *Connecticut*. Scott Armstrong performed some of the initial analysis of the CODAR data. We also thank the Block Island Southeast Light Foundation, the Montauk Point Lighthouse Museum, the Rhode Island Department of Environmental Management, and the U.S. Coast Guard for granting permission to utilize their properties for the CODAR installations.

References

Barrick, D. E., and B. J. Lipa (1986), Correcting for distorted antenna patterns in CODAR ocean surface measurements, *IEEE J. Oceanic Eng.*, *OE-11*, 304–309.

Barrick, D. E., and B. J. Lipa (1997), Evolution of bearing determination in HF current mapping radars, *Oceanography*, *10*, 72–75.

Barrick, D. E., J. M. Headrick, R. W. Bogle, and D. D. Crombie (1974), Sea backscatter at HF: Interpretation and utilization of the echo, *Proc. IEEE*, *62*, 673–680.

Barrick, D. E., M. W. Evans, and B. L. Weber (1977), Ocean surface currents mapped by radar, *Science*, *198*, 138–144.

Beardsley, R. C., and W. C. Boicourt (1981), On estuarine and continental shelf circulation in the Middle Atlantic Bight, in *Evolution of Physical*

Oceanography, edited by B. A. Warren and C. Wunsch, pp. 198–233, MIT Press, Cambridge, Mass.

Beardsley, R. C., and B. Butman (1974), Circulation on the New England continental shelf: Response to strong winter storms, *Geophys. Res. Lett.*, *1*, 181–184.

Beardsley, R. C., D. C. Chapman, K. H. Brink, S. R. Ramp, and R. Schlitz (1985), The Nantucket Shoals Flux Experiment (NSFE79): I. A basic description of the current and temperature variability, *J. Phys. Oceanogr.*, *15*, 713–748.

Bowman, M. J., and W. E. Esaias (1981), Fronts, stratification, and mixing in Long Island and Block Island Sounds, *J. Geophys. Res.*, *86*, 4260–4264.

Chapman, R. D., L. K. Shay, H. C. Graber, J. B. Edson, A. Karachintsev, C. L. Trump, and D. B. Ross (1997), On the accuracy of HF radar surface current measurements: Intercomparison with ship-based sensors, *J. Geophys. Res.*, *102*, 18,737–18,748.

Chuang, W. S., D. P. Wang, and W. C. Boicourt (1979), Low-frequency current variability on the southern Mid-Atlantic Bight, *J. Phys. Oceanogr.*, *9*, 1144–1154.

Codiga, D. L., and A. E. Houk (2002), Current profile timeseries from the FRONT moored array, technical report, Dep. of Mar. Sci., Univ. of Conn., Storrs.

Codiga, D., and L. Rear (2004), Observed tidal currents outside Block Island Sound: Offshore decay and effects of estuarine outflow, *J. Geophys. Res.*, *109*, C07S05, doi:10.1029/2003JC001804, in press.

Codiga, D. L., J. A. Rice, and P. S. Baxley (2004), Networked acoustic modems for real-time data delivery from distributed moorings in the coastal ocean: Initial system development and performance, *J. Atmos. Oceanic Technol.*, *21*(2), 331–346.

Conkright, M. E., et al. (1998), World Ocean Database 1998: Documentation and quality control, version 1.2, *Internal Rep. 14*, Natl. Oceanogr. Data Cent., Silver Spring, Md.

Csanady, G. T. (1979), The pressure field along the western margin of the North Atlantic, *J. Geophys. Res.*, *84*, 4905–4915.

Csanady, G. T. (1982), *Circulation in the Coastal Ocean*, D. Reidel, Norwell, Mass.

Kincaid, C., R. A. Pockalny, and L. M. Huzzey (2003), Spatial and temporal variability in flow at the mouth of Narragansett Bay, *J. Geophys. Res.*, *108*(C7), 3218, doi:10.1029/2002JC001395.

Large, W. G., and S. Pond (1981), Open ocean momentum flux measurements in moderate to strong winds, *J. Phys. Oceanogr.*, *11*, 324–336.

Lipa, B. J., and D. E. Barrick (1983), Least-squares methods for the extraction of surface currents from CODAR crossed-loop data: Application at ARSLOE, *IEEE J. Oceanic Eng.*, *OE-8*, 226–253.

Longuet-Higgins, M. S. (1969), On the transport of mass by time-varying ocean currents, *Deep Sea Res.*, *16*, 431–447.

Mayer, D. A., D. V. Hansen, and D. A. Ortman (1979), Long-term current and temperature observations on the Middle Atlantic shelf, *J. Geophys. Res.*, *84*, 1776–1792.

Press, W. H., S. A. Teukolsky, W. T. Vetterling, and B. P. Flannery (1992), *Numerical Recipes in FORTRAN: The Art of Scientific Computing*, 2nd ed., Cambridge Univ. Press, New York.

Stewart, R. H., and J. W. Joy (1974), HF radio measurements of ocean surface currents, *Deep Sea Res.*, *21*, 989–1016.

Ullman, D. S., and P. C. Cornillon (1999), Satellite-derived sea surface temperature fronts on the continental shelf off the northeast U.S. coast, *J. Geophys. Res.*, *104*, 23,459–23,478.

Ullman, D. S., and P. C. Cornillon (2001), Continental shelf surface thermal fronts in winter off the northeast U. S. coast, *Cont. Shelf Res.*, *21*, 1139–1156.

Visser, A. W., M. J. Bowman, and W. R. Crawford (1990), Dynamics of tidally forced basin-wide coastal eddies, in *Residual Currents and Long-Term Transport*, edited by R. T. Cheng, pp. 64–78, Springer-Verlag, New York.

Wilson, R. E. (1976), Gravitational circulation in Long Island Sound, *Estuarine Coastal Mar. Sci.*, *4*, 443–453.

D. L. Codiga, Department of Marine Sciences, University of Connecticut, 1080 Shennecossett Road, Groton, CT 06340, USA. (d.codiga@uconn.edu)

D. S. Ullman, Graduate School of Oceanography, University of Rhode Island, 215 South Ferry Road, Narragansett, RI 02882, USA. (d.ullman@gso.uri.edu)